Supplementary Information (SI) for Journal of Materials Chemistry C.

Supplemental Material

Correlation between Domain Structure Dynamics and Electromechanical Behavior in Sn-doped $BaTiO_3$

Viktoria Kraft,[1,*] Maria Rita Cicconi,[1] Subhajit Pal,[2] Michel Kuhfuß,[1] Neamul H. Khansur,[1,3] Alexander Martin,[4] Koji Kimura,[5] Yasuhiro Takabayashi,[5] Ko Mibu,[5] Koichi Hayashi,[5] Joe Briscoe,[2] Kyle G. Webber[1]

[1]Department of Materials Science and Engineering, Friedrich-Alexander-Universität Erlangen-Nürnberg, Erlangen 91058, Germany
[2]School of Engineering & Materials Science, Queen Mary University of London, London E1 4NS, United Kingdom
[3]Department of Materials Science & Engineering, Case Western Reserve University, Cleveland OH, 44106
[4]Department of Life Science and Applied Chemistry, Nagoya Institute of Technology, Nagoya, Aichi 466-8555, Japan
[5]Department of Physical Science and Engineering, Nagoya Institute of Technology, Nagoya, Aichi 466-8555, Japan

[*]corresponding author: viktoria.kraft@fau.de

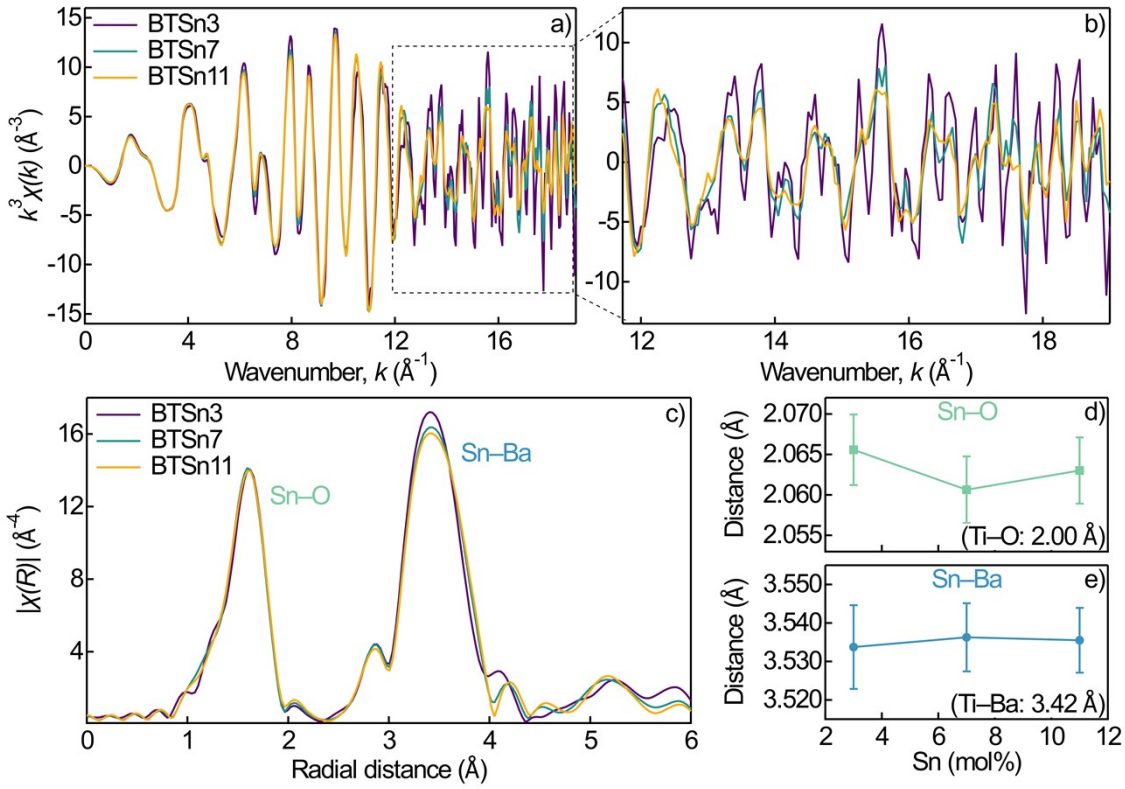

Figure S1. Sn K-edge XAFS with (a) k^3-weighted oscillation function, (b) enlarged high-k region of the oscillation function, (c) χ(R), the magnitude of the phase-corrected Fourier transform of $k^3\chi(k)$, (d) Sn-O bond lengths, and (e) Sn-Ba bond lengths.

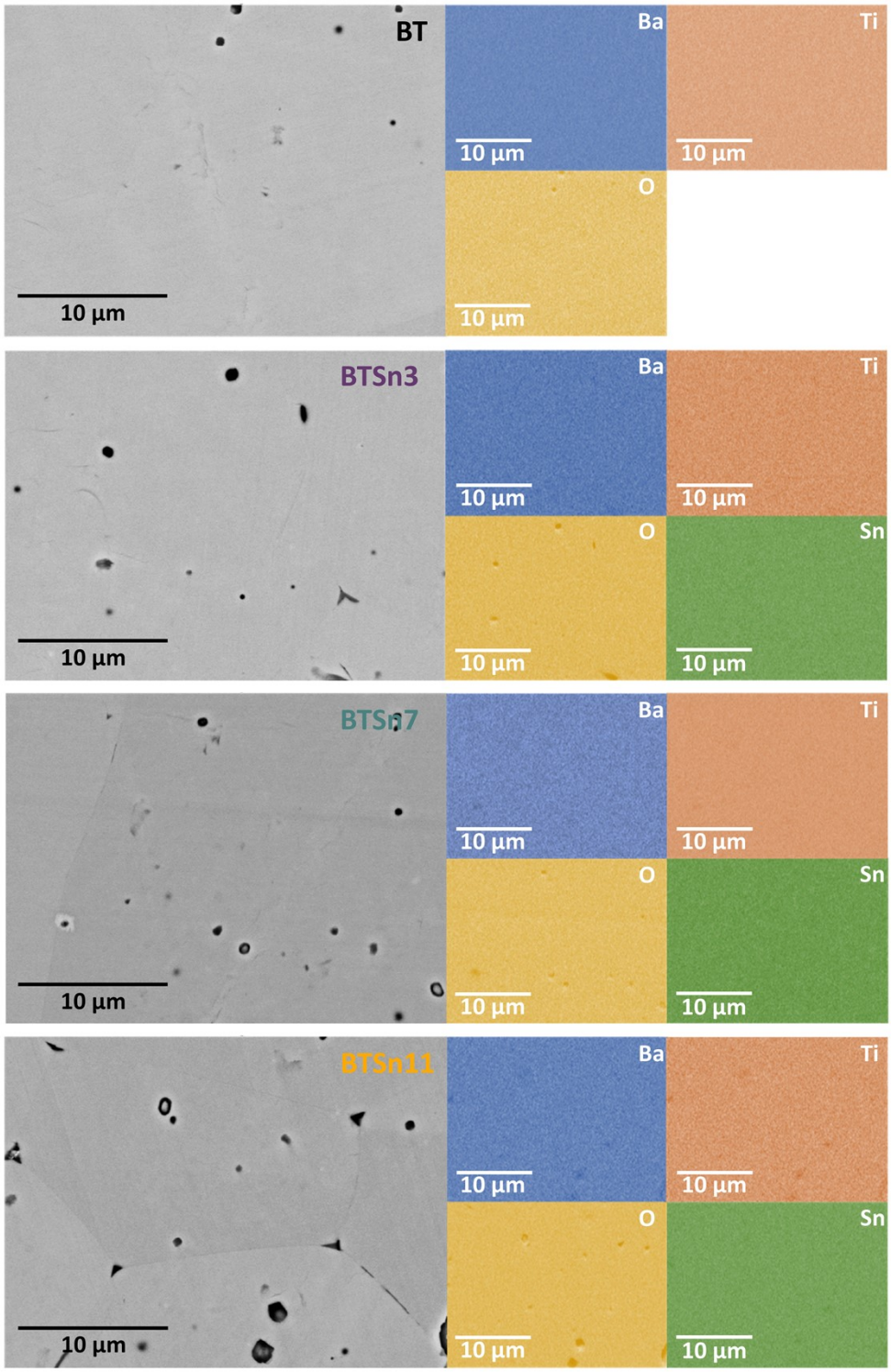

Figure S2. FESEM images and EDS maps of BTSn100*x* samples.

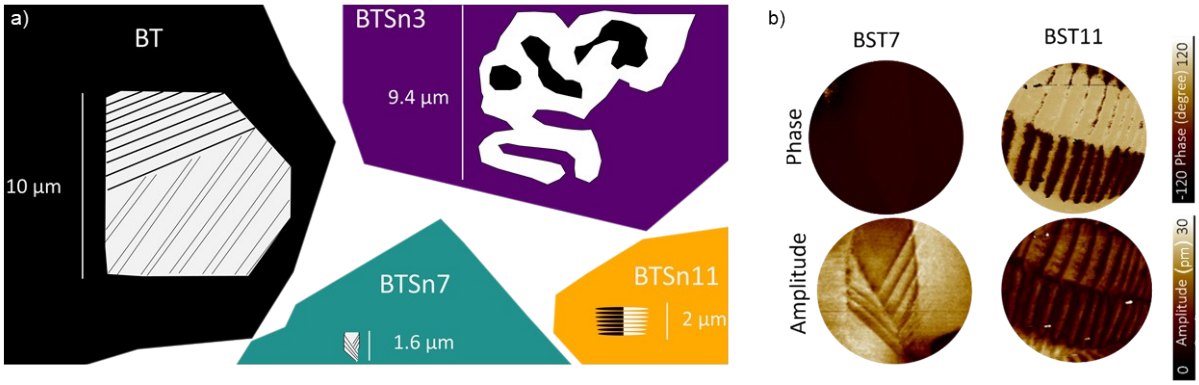

Figure S3. a) Schematic diagram of domain morphology and size evolution, and b) enlarged piezoresponse force microscopy amplitude and phase images of BTSn7 and BTSn11 showing herringbone-like domain pattern.

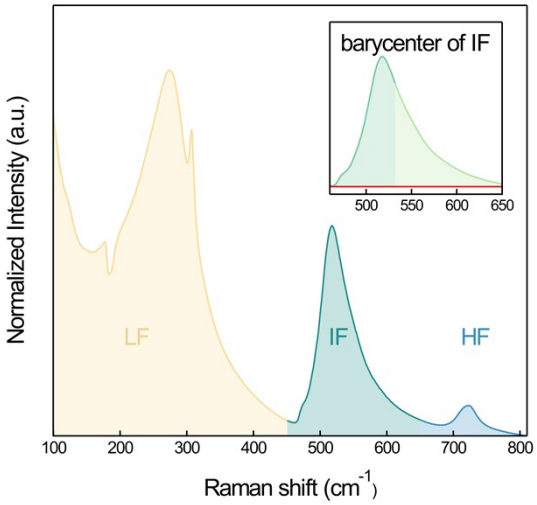

Figure S4. Typical Raman spectrum of BT with mode and frequency range assignment and visualization of a centroid determination of overlapping modes.

Table S1. Raman modes and corresponding symmetry assignments for tetragonal BT, based on previous reports[48,66,87,88].

Range	BT	Mode
LF	180	LO
	270	A_1(TO)
	307	E+B_1
IF	470	LO
	510	A_1(TO)
HF	715	LO

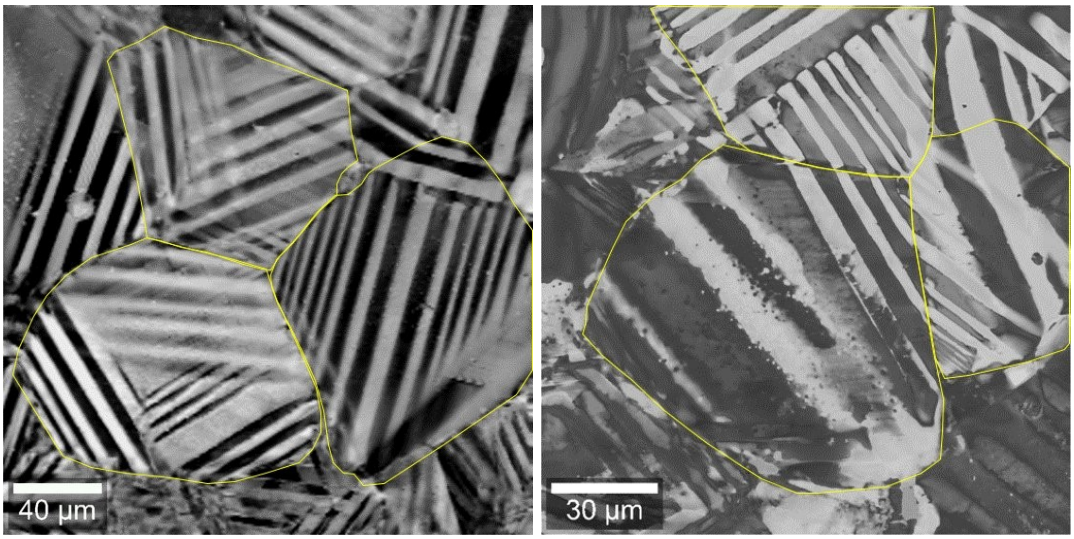

Figure S5. Reconstructed Raman hyperspectral images with marked areas used to determine the average domain wall density.

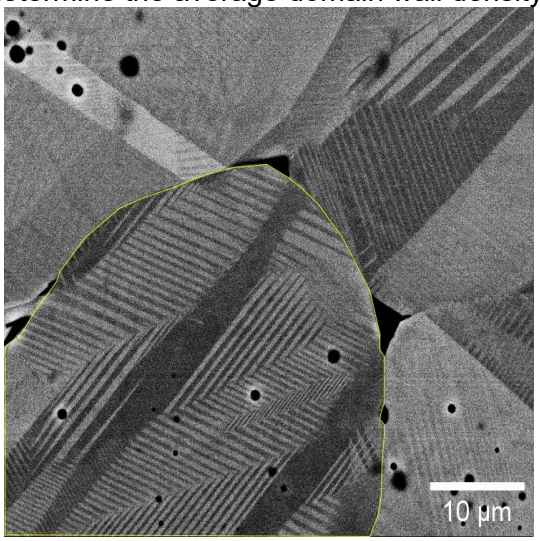

Figure S6. Scanning electron microscopy image with marked area used to determine the average domain wall density.

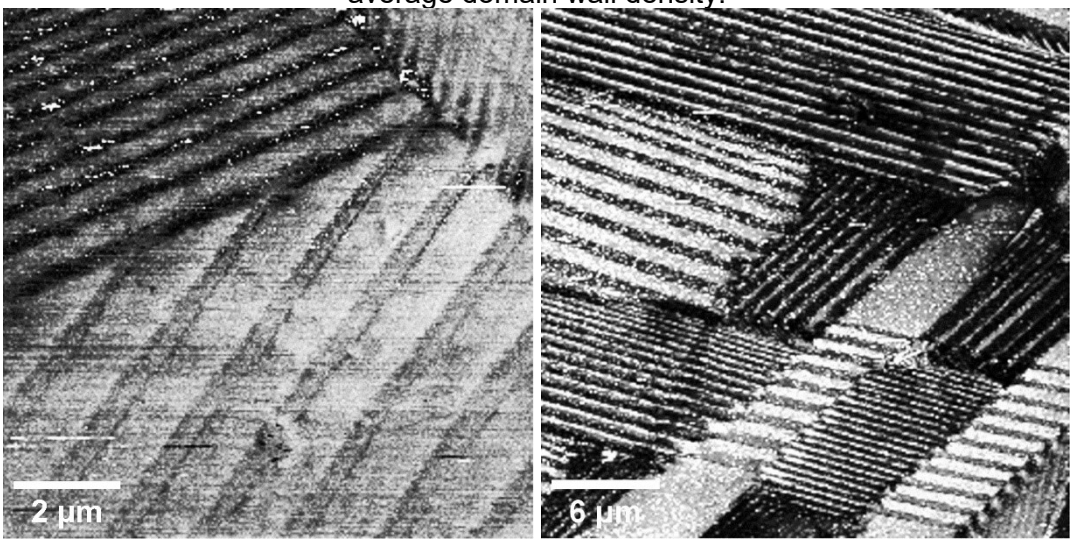

Figure S7. Piezoresponse force microscopy images used to determine the average domain wall density.

It should be noted that different areas and approaches were used to determine the domain wall density for the various measurement techniques. For Raman and SEM images, only selected yellow-marked areas were analyzed, as it was difficult to identify all domain walls across the full image, for example, due to focus deviations. In contrast, for PFM, the entire image could be used. The obtained values should be interpreted cautiously and considered more as a guideline rather than absolute values. The standard deviation was calculated for Raman between the different marked areas and for PFM between different images. For SEM, only a single area was analyzed, so no standard deviation was determined. The aim was to assess the comparability of the different techniques and identify potential trends rather than to determine absolute values.

Table S2. Calculated average domain wall density for the different microscopic methods.

Method	Average domain wall density (μm^{-2})
Raman	0.005±0.003
SEM	0.367
PFM	0.377±0.13

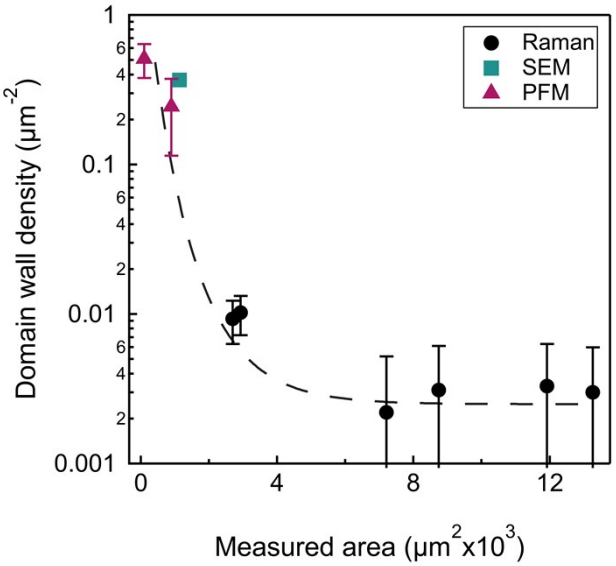

Figure S8. Domain wall density as a function of measured area with guide for the eye (dashed line), demonstrating the decrease in resolvable domain walls with reduced spatial resolution and magnification, as a consequence of larger sampled areas, across different microscopy techniques.